Microstreamer dynamics during plasma remediation of NO using atmospheric pressure dielectric barrier discharges

Ann C. Gentile[a] and Mark J. Kushner[b]
Department of Electrical and Computer Engineering, University of Illinois, Urbana, Illinois 61801

(Received 11 September 1995; accepted for publication 18 December 1995)

Environmental concerns have resulted in the need for alternative energy efficient methods for the removal of oxides of nitrogen (N_xO_y) from atmospheric gas streams and among those techniques is plasma remediation. The devices typically used as plasma sources (corona and dielectric barrier discharges) operate in a filamentary mode which produces radicals and gas heating in narrow channels. Transport of radicals and products is therefore an important consideration in optimizing their efficiency. In this article we describe and present results for a radially dependent model of N_xO_y remediation in dielectric barrier discharges. We examine the consequences of localized energy deposition, and diffusive and advective radial transport, and determine how these spatial dependencies affect the energy efficiencies for N_xO_y removal. Local energy deposition in the streamer can produce high temperatures initiating advection and facilitating production of NO through $N+O_2 \rightarrow NO+O$. Diffusion of NO into the streamer region from the bulk gas and advective transport of N outward into the bulk gas increase remediation of N_xO_y by channeling N into remediation, $NO+N \rightarrow N_2+O$, rather than radical reassociation, $N+N+M \rightarrow N_2+M$. Remediation efficiency generally decreases with increasing energy deposition due to the reassociation reaction and formation of NO. Transport of N out of and NO into the streamer region reduces this effect.
 [S0021-8979(96)03207-5]

I. INTRODUCTION

Increasing concern over the emission of hazardous gases into the atmosphere has motivated research into environmentally acceptable and economically viable methods to remediate toxins from atmospheric pressure gas streams. Plasma remediation is one technique which has been investigated for remediation of SO_2 and oxides of nitrogen (N_xO_y) from combustion of fossil fuels, and for remediation of volatile organic compounds.[1–5] Plasma remediation is attractive due to its high efficiency of producing oxidizing or reducing radicals, and the ability to process the toxins at low average gas temperatures. The dielectric barrier discharge (DBD) is one candidate for the plasma generator in these devices.[6–8] The plasma in DBDs typically consists of an array of filamentary or ''microstreamer'' discharges. Each microstreamer is between tens and hundreds of microns in diameter and lasts for tens to hundreds of ns. They are produced with an area density of a few tens of cm^{-2} at a repetition rate of between tens of Hz to a few kHz. The radicals produced by a single microstreamer process a fraction of the toxin in a small volume. Remediation of the entire toxic gas inventory is obtained by repetitive operation of the device which, on the average, processes each subvolume of gas by many microstreamer pulses.[5,9,10]

The filamentary plasma in DBDs (and corona discharges) deposits power and generates radicals by electron impact in narrow channels. For a given volume averaged power deposition, gas temperature, and radical densities are higher in the microstreamers than in a device in which power is uniformly deposited. There are at least two consequences of this nonuniform power deposition. First, for sufficiently high energy deposition per pulse, gas heating on the axis of the microstreamer can initiate advection and rarefaction as observed in spark gaps and high pressure pinch discharges.[11] Second, the local power deposition generates radicals in confined regions. Therefore transport of reactants and products into and out of the streamer region may impact the energy efficiency of the process.

In a previous work, we presented the results from a computational study of the plasma remediation of N_xO_y using repetitively pulsed DBDs in which all quantities were treated as volume averaged.[10] The major reaction pathways in remediation of N_xO_y were discussed and scaling laws for energy efficiency were presented. In this work we extend the analysis by including radial hydrodynamics in the vicinity of a microstreamer following a current pulse. In doing so, we investigate the effect of local power deposition, and reactant and product transport on the remediation process.

In Sec. II we describe our computer model for the DBD. In Sec. III we discuss the major reactions that determine the energy efficiency of remediation, and the effect of diffusion on the remediation efficiency. The consequences of diffusive and advective transport on remediation and energy efficiency are discussed in Sec. IV, followed by our concluding remarks in Sec. V.

II. DESCRIPTION OF THE MODEL

To investigate the volumetric plasma kinetics and transport phenomena in DBD remediation, we have developed a one-dimensional, radially dependent model. The simulation consists of a circuit model, a solution of Boltzmann's equa-

[a]Present address: Sandia National Laboratory, Livermore, CA 94551. Electronic mail: gentile@dancer.ca.sandia.gov
[b]Author to whom correspondence should be addressed. Electronic mail: mjk@uiuc.edu

tion for the electron energy distribution, a plasma chemistry model, and a transport model. The circuit model provides E/N (electric field/gas number density) in the plasma which is used as input to the solution of Boltzmann's equation. Boltzmann's equation is solved using a two term spherical harmonic expansion to determine the electron energy distributions from which electron impact rate coefficients are generated. The transport model further updates the species densities from the plasma chemistry module accounting for diffusion and advection.

The plasma chemistry, Boltzmann and circuit portions of the model are essentially the same as discussed in Ref. 10. The plasma chemistry model solves for the local densities of species. There are 331 reactions and 56 species considered in the full reaction set of the plasma chemistry model, and these reactions are discussed in Refs. 10 and 12. There are 43 electron impact processes in the plasma chemistry model which obtain their rate coefficients from the solution of Boltzmann's equation. A reduced reaction set of 160 reactions and 33 species is used in the full advective model to reduce computing time. The vast majority of the pertinent physics is captured with the reduced reaction set.

In the transport module, we represent the DBD as a matrix of equispaced radially symmetric streamers. The total discharge area is divided into square regions each having a streamer at its center. Using reflecting boundary conditions we then simulate a single repetitively pulsed streamer as representative of the device as a whole. In the model the streamer occurs in the same location in each pulse. These assumptions are approximations since, in actual devices, the streamers will have axial variations, and will not be equally spaced.[6–8,13,14] The streamers are initiated, however, at approximately the same voltage, and so may occur close enough in time for the streamers to begin nearly simultaneously. Also, charging of the dielectric, thereby locally reducing the required avalanche voltage, and defects in the surface can lead to electric field enhancements that may cause the streamers to occur preferentially in the same location each current pulse.

For computational purposes, the streamer is assumed to be radially symmetric and its volume is discretized using finite difference techniques as concentric cylinders centered on the streamer. The exception is that the outermost computational element is actually a square with a circular inner surface. The radial mesh has continuously varying spacing to allow resolution of both the streamer (typically between a few microns and tens of microns in diameter) and interstreamer spacing (mm to cm). We typically use 250 radial mesh points in a full advective model. In the circuit model, each individual computational element (a cylindrical shell) is treated as a resistor and the plasma is represented as a set of resistors in parallel. The streamer is shut off after a fixed energy deposition as opposed to being extinguished by the charge buildup on the dielectric. This choice was made to enable comparison of cases based upon a specified energy deposition.

In order to study the contributions of diffusion and advection separately, we employed two variations of the transport model. In the first, transport is limited to diffusion alone while in the second transport is due to both diffusion and advection. The purpose of considering only diffusive transport is to investigate phenomena resulting only from gradients in production of reactants. Such an approach is strictly applicable only to low energy deposition where the temperature rise and pressure gradients are small. Some of the cases presented in Sec. III, where we discuss results from the model including only diffusion may, in fact, require inclusion of advection to accurately capture the real behavior of the system. Spatial dependencies due to both diffusion and advection and their effects are discussed in Sec. IV.

The time rates of change of species densities and gas temperature in the case including diffusion only are calculated from

$$\frac{dN_i}{dt} = \nabla \cdot (D_i \nabla N_i) + \left(\frac{\partial N_i}{\partial t} \right)_p , \tag{1}$$

$$\frac{d(\rho c_v T)}{dt} = j \cdot E + \nabla \cdot \kappa \nabla T. \tag{2}$$

D_i is the diffusion constant for species i, ρ is the mass density, c_v is the heat capacity, j is the current density, E is the electric field, and κ is the thermal conductivity. Diffusion constants were estimated by

$$D_i = \frac{1}{\Sigma_j \dfrac{1}{D_{ij}}}, \tag{3}$$

where D_{ij} is the binary diffusion coefficient between species i and j. Binary diffusion coefficients were calculated based on Lennard-Jones σ radii.[15] The values we used for σ are listed in Ref. 12. Since the change in enthalpy due to chemical reactions is small, that term has been ignored. $(\partial N_i/\partial t)_p$ represents the change in species density due to the local plasma kinetics. We are not tracking the densities of vibrationally excited species. As a result the power which is channeled into vibrational excitation appears as gas heating, which implies rapid vibrational relaxation. One can therefore consider this analysis a worst case. To test this assumption, we performed extensive parameterizations of the model for current pulses through N_2 and N_2/O_2 gas mixtures.[16] We tracked the pertinent vibrational and electronic states, and their contributions to the enthalpy. We found that at the high current densities of interest, the electron density is sufficiently large that superelastic collisions quench vibrational and electronic states rapidly. As a result, the energy storage in those species is minimal.

The species densities are updated in two stages. First, the plasma chemistry model independently calculates the change in species densities and gas temperature due to the local kinetics for each mesh point using a third-order Runge–Kutta scheme. Following the update of the local kinetics, the densities for all species and the gas temperature at all locations are implicitly updated for diffusive transport. This technique was chosen because significant changes in species densities due to kinetics typically occur on much shorter time scales than do changes in densities due to diffusion. The advantage of this technique is that the local kinetics in each region can

be independently calculated using a separate time step, which is short in the streamer (<1 ns during the current pulse) and long in the outer regions. The transport derivatives were expressed using central finite differences. This produces a tridiagonal matrix for each species density as a function of radius. The implicit update for diffusive transport is then accomplished by a simple matrix inversion.

When including both diffusive and advective transport, species densities are determined by

$$\frac{dN_i}{dt} = \nabla \cdot [D_i \rho \nabla (N_i/\rho) - N_i \mathbf{v}] + \left(\frac{\partial N_i}{\partial t} \right)_p , \tag{4}$$

where ρ is the mass density and $\mathbf{v}$ is the average advective velocity in the radial direction. The advective velocity is determined from solution of the Navier–Stokes equations

$$\frac{\partial \rho}{\partial t} = -\nabla \cdot (\rho \mathbf{v}), \tag{5}$$

$$\frac{\partial (\rho \mathbf{v})}{\partial t} = -\nabla P - \nabla \cdot (\rho \mathbf{v}\mathbf{v}) - \nabla \cdot \bar{\bar{\tau}}, \tag{6}$$

$$\frac{\partial (\rho c_v T)}{\partial t} = j \cdot E - \nabla \cdot (\rho \mathbf{v} c_v T) - P \nabla \cdot \mathbf{v} + \nabla \cdot \kappa \nabla T + 2\mu (\nabla \cdot \mathbf{v})^2, \tag{7}$$

where P is the thermodynamic pressure, $\bar{\bar{\tau}}$ is the viscosity tensor, and μ is the velocity.

In integrating Eq. (4), the densities are first independently updated at each mesh point due to the local kinetics. The densities are then updated due to advection using the single advective velocity for all species. Finally, these densities are updated based on diffusion which does not change ρ. In practice, the advective update for the species densities is performed simultaneously with integration of the Navier–Stokes equation. This is necessary to capture the real time changes in $\mathbf{v}$ required to maintain mass conservation.

The Navier–Stokes equations are integrated and advection is included in Eq. (4), until pressure gradients and the advective velocity initiated by the streamer damp to sufficiently small values. At that time, typically 1 ms after the current pulse, advection is ignored and species densities and temperature are determined by Eqs. (1) and (2) for the remainder of the interpulse period (up to 1 s.).

In the results which follow, we examined a single streamer. For the diffusion only calculations, the plasma channel diameter is initially 40 μm. The computational volume is 0.02×0.02 cm^2 and 3 mm in depth. For the full advective calculations the plasma channel is ≈ 60 μm diameter. The computational volume is 0.8×0.8 cm^2 in cross sectional area and 3 mm in depth. The streamer therefore occupies a small fraction of the total volume particularly in the latter case. The large disparity in size was a deliberate choice to minimize edge effects. The remediation we quote therefore appears artificially low due to the large ratio in volumes. Note, however, that plasma remediation results from a series of current pulses (tens of Hz to a few kHz for a few seconds of residence time), each removing a fraction of the initial density of NO. For example, a processing rate of 10^6 microstreamers/cm^2 s (repetition rate 10^3 Hz) has been measured for DBD processing of volatile organic compounds.[17]

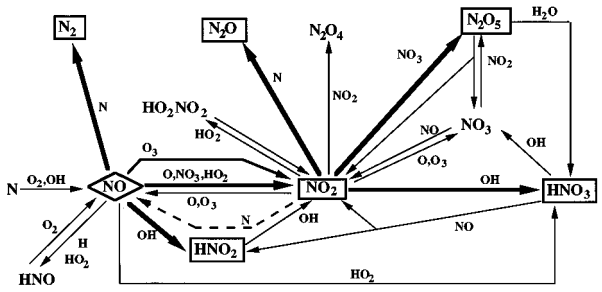

FIG. 1. Dominant reaction pathways in the plasma remediation of NO. The initial toxin is shown by a diamond. The major products (NO_2, N_2O, N_2O_5, N_2, HNO_2, HNO_3) are boxed. The radicals assisting each reaction are shown next to the corresponding arrow. The reduction reaction of NO with N is the dominant reaction pathway for remediation. The back reaction of N with NO_2, and the interpulse reaction of O_3 with NO_2 replenish NO.

For the results which follow, for parametric purposes we have specified a given energy deposition which will produce a desired on axis temperature rise. Obtaining this energy deposition in any given device depends on practical matters such as the format of the applied voltage pulse, the thickness of the dielectric and its permittivity. To address this issue we performed parameterizations for current pulses through N_2 while varying the dielectric properties using a square wave voltage pulse.[16] We found that the energy deposition and on axis temperature rise increased nearly linearly with increasing capacitance of the dielectric, ϵ_d/L (ϵ_d=permittivity, L=thickness of the dielectric). For example, the peak on axis temperature rise is $\approx$50 K for a dielectric capacitance of 140 pF/cm^2 and voltage of 12 kV for a 0.2 cm gap. As expected the temperature rise increases with the square of the line voltage.

III. DIFFUSIVE TRANSPORT AND RADIALLY DEPENDENT KINETICS

The dominant reaction pathways in the plasma remediation of NO are shown in Fig. 1. A detailed discussion of those pathways appears in Refs. 10 and 12, and so only a review of the important reactions pertinent to this work will follow.

Plasma remediation of NO in DBDs is initiated by electron impact dissociation of N_2, O_2, and H_2O generating N, O, and OH, respectively. Due to the filamentary nature of the plasma, these radicals are produced in narrow channels. Under the conditions studied in this work ($N_2/O_2/H_2O$=85/5/10, 500 ppm NO, 400 K, 1 atm), the reduction reaction[18]

$$\mathrm{NO + N \rightarrow N_2 + O}, \quad k_8 = 3.1 \times 10^{-11} (T/300)^{1/2} \ \mathrm{cm^3\ s^{-1}} \tag{8}$$

is the primary remediation pathway for NO. Since remediation of NO dominantly is through this reaction, we will concentrate on it and on reactions that are competing processes for N. The major competing process for N atoms is the radical reassociation reaction[18]

$$\mathrm{N + N + M \rightarrow N_2 + M},$$

$$k_9 = 3.9\times10^{-33}(T/300)^{-3/2}\ \text{cm}^6\,\text{s}^{-1}. \tag{9}$$

At atmospheric pressure, the reassociation reaction competes with remediation when

$$[N] > \frac{[\text{NO}]k_8}{[\text{M}]k_9} \approx 500\ [\text{NO}]. \tag{10}$$

Therefore when NO is depleted and [N] is large, conditions obtained at high power late in the remediation process, reassociation of N is the dominant loss process. This condition may also occur locally in the center of the microstreamer. If not initially present, NO_2 is produced by[19]

$$\begin{aligned} &\text{NO}+\text{O}+\text{M}\rightarrow\text{NO}_2+\text{M},\\ &k_{11}\approx 9.1\times10^{-28}T^{-1.6}\ \text{cm}^6\,\text{s}^{-1},\quad (\text{M}=\text{N}_2). \end{aligned} \tag{11}$$

N atoms are then consumed by the back reaction[18]

$$\begin{aligned} &\text{NO}_2+\text{N}\rightarrow\text{NO}+\text{NO},\\ &k_{12}=6\times10^{-13}(T/300)^{1/2}\ \text{cm}^3\,\text{s}^{-1}, \end{aligned} \tag{12}$$

which converts NO_2 back into NO. This process is generally slower than that of Eq. (8) due to both the lower rate coefficient and lower density of NO_2. Oxygen atoms produced by electron impact of O_2 are dominantly lost by formation of ozone producing densities of $O_3 > 10^{16}$ cm^{-3}. Most of the remediation of NO at long times after the current pulse ($t > 10^{-4}$ s) results from reactions of NO with O_3:[20]

$$\begin{aligned} &\text{NO}+\text{O}_3\rightarrow\text{NO}_2+\text{O}_2,\\ &k_{13}=2\times10^{-12}\exp(-1400/T)\ \text{cm}^3\,\text{s}^{-1}. \end{aligned} \tag{13}$$

This process removes NO without changing the net amount of N_xO_y.

Finally, in the presence of water vapor, NO and NO_2 can be converted to acidic products by reaction with OH:[19]

$$\begin{aligned} &\text{NO}+\text{OH}+\text{M}\rightarrow\text{HNO}_2+\text{M},\\ &k_{14}=6.5\times10^{-25}T^{-2.4}\ \text{cm}^6\,\text{s}^{-1}, \end{aligned} \tag{14}$$

$$\begin{aligned} &\text{NO}_2+\text{OH}+\text{M}\rightarrow\text{HNO}_3+\text{M},\\ &k_{15}=3.3\times10^{-23}T^{-2.6}\ \text{cm}^6\,\text{s}^{-1}. \end{aligned} \tag{15}$$

The volume averaged densities of NO and N_xO_y during and following a single current pulse are shown in Fig. 2 as a function of time (1 ppm$=1.8\times10^{13}$ cm^{-3}). The initial conditions are $N_2/O_2/H_2O=85/5/10$ with 500 ppm NO, and a gas temperature of 400 K at 1 atm. The energy deposition in the streamer (radius ≈ 10 μm) is roughly 125 mJ/cm^3 which corresponds to 1 mJ/cm^3 averaged over the entire computational region. The three characteristic time regimes during remediation (discussed in Ref. 10) are the pulse, post pulse remediative period (PPRP), and interpulse (IP). The current pulse lasts $\sim10^{-8}$ s. During this time, the N, O, and OH radicals are formed from N_2, O_2, and H_2O by electron impact processes. The PPRP is from the end of the current pulse to $\sim10^{-4}$ s. During this time, NO is converted into the major products (N_2, NO_2, N_2O, N_2O_5, HNO_2, NHO_3) by reactions with the radicals. The PPRP ends when the radicals are depleted. Finally the IP lasts from the end of the PPRP to the onset of the next current pulse. During this latter time the only major process with respect to remediation is reaction of NO with O_3 [Eq. (13)]. The NO density changes while the inventory of N_xO_y does not.

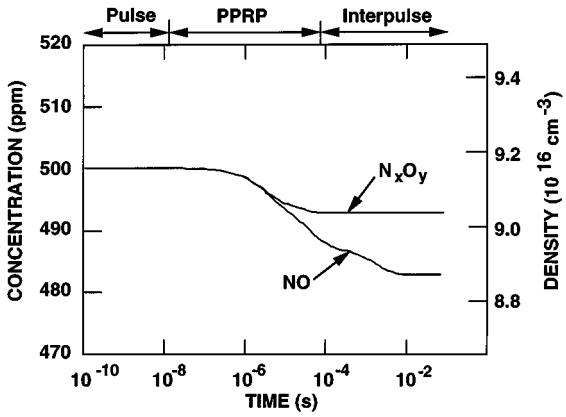

FIG. 2. Volume averaged densities of NO and N_xO_y as a function of time. The initial gas mixture is $N_2/O_2/H_2O=85/5/10$ with 500 ppm of NO (1 atm, 400 K). The streamer–volume averaged energy deposition is 125 mJ/cm^3. The durations of the current pulse, the PPRP, and interpulse periods are shown at the top of the figure.

The electron, N and O_3 densities during and following the current pulse are shown in Fig. 3. For these results transport is by diffusion only. Since the rate of ambipolar diffusion is commensurate to dissociative recombination, the electrons do not diffuse far beyond the edge of the streamer region. The electron avalanche produces primary radicals N, OH, and O during the pulse. Rapid consumption of N and OH by remediative and radical–radical recombination reactions prevents them from diffusing far beyond the streamer. N atoms are exhausted after a few μs. The rapid formation of O_3 from O atoms similarly prevents O from diffusing far beyond the streamer. The relatively low reactivity of O_3, however, results in a long diffusion length. Therefore O_3 is fairly uniformly distributed at the time that it reacts with NO [Eq. (13)]. This occurs during the IP, roughly after 10^{-4} s. The O_3 concentration initially builds up in the streamer region due to the large concentration of O atoms generated by electron impact reactions and radially diffuses outward [see Fig. 3(c)]. As the O atoms are depleted, production of O_3 slows and diffusion levels the profile.

The density of NO during remediation is shown in Fig. 4. Remediation of NO begins in the streamer region by reduction reactions with N atoms. The density of NO is depleted on axis where the density of N atoms is large. At this time ($\lesssim10^{-6}$ s) the rate of remediation exceeds the rate of diffusion which replenishes NO from larger radii. The N atoms are exhausted at times of 10^{-6}–10^{-5}, and remediation of NO by reduction slows. Diffusion of NO from outer regions then fills in the depleted NO profile until a uniform distribution is reached, roughly at the end of the PPRP. The NO then decreases uniformly in space due to reaction with O_3 which produces NO_2 [Eq. (13)].

Diffusion of NO from larger radii into the streamer region can affect, and in most cases increase, the efficiency of remediation in the streamer region where the density of N is

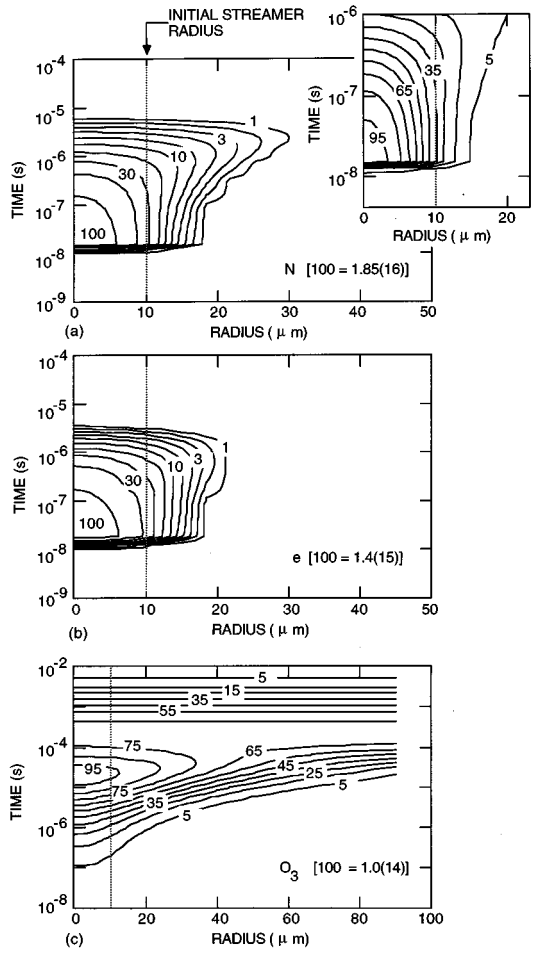

FIG. 3. Species densities (cm^{-3}) for a current pulse having only diffusive transport for the conditions of Fig. 2. (a) N, (b) electrons, and (c) O_3. The inset for the N atoms density shows more detail at early times. The contours are labeled with the percentage of the maximum value indicated. The electron density quickly decays after the current pulse. The electrons do not diffuse far beyond the streamer region (indicated by the dashed line). The primary radical N is formed in and near the streamer during the pulse but reacts with NO prior to diffusing far beyond the streamer. The secondary radical O_3 builds in and near the streamer region and diffuses outward. O_3 is uniformly distributed at the time of its reaction with NO.

high. If the ratio of N/NO is large, recombination reactions [Eq. (9)] dominate over remediation reactions [Eq. (8)] and the efficiency will be low. This is the case in the streamer region shortly after the current pulse when the density of N is large and NO may be depleted. Diffusion of NO into the streamer reduces the N/NO ratio and so increases the fraction of N that will be used in remediation. The efficiency of remediation can therefore increase.

The localized energy deposition in the streamer region, which produces high gas temperatures can also affect the efficiency, generally lowering it, by allowing reactions having large activation energy barriers to proceed. In particular, the reaction[21]

$$N+O_2 \rightarrow NO+O,$$

$$k_{16}=4.4\times 10^{-12}\exp(-3220/T)\ \ \mathrm{cm^3\,s^{-1}} \qquad (16)$$

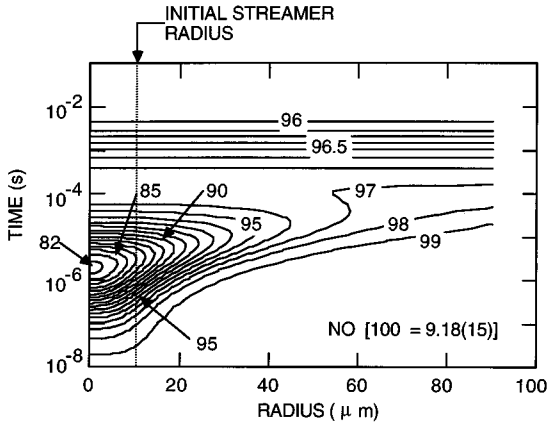

FIG. 4. NO density for the conditions of Fig. 2. The contours are labeled with the percentage of the maximum value indicated. Remediation begins in the streamer region due to the local generation of N and O ($t<10^{-6}$ s). The rate of remediation exceeds diffusion during this time. Remediation continues until the end of the PPRP ($t<10^{-4}$ s); however, diffusion from the outer regions fills in the profile until a uniform NO distribution is reached. Finally NO decreases uniformly during the interpulse period ($t>10^{-4}$ s) by reaction with ozone since NO and O_3 are uniform at this time.

provides a source of NO which decreases the net amount of remediation. This effect is more detrimental with increasing energy deposition since there is a commensurate increase in temperature. The temperature rise which enables this reaction would also rarefy the channel and produce advection. To isolate the effect of this reaction we suppressed advection and parameterized the energy deposition. These results are shown in Fig. 5 where NO densities for streamer volume averaged energy depositions of 125, 255, and 380 mJ/cm^3 are shown shortly after the end of the pulse. These energy depositions produce temperatures in the streamer of 550, 700, and 850 K. For low energy deposition, where the temperatures and radical densities are relatively low, the largest

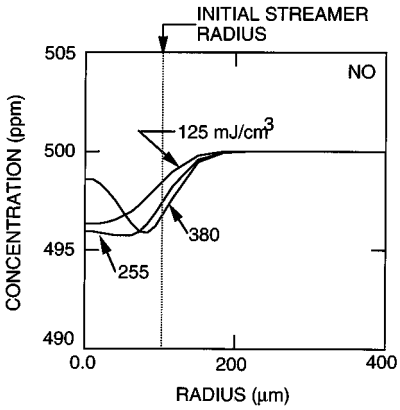

FIG. 5. NO densities for streamer–volume averaged energy depositions of (a) 125, (b) 255, and (c) 380 mJ/cm^3. Larger densities of primary radical densities at larger energy depositions increase the rate of NO remediation. However, the higher gas temperatures at large energy deposition also increase NO generating reactions with high activation energies such as $N+O_2 \rightarrow NO+O$. These effects are greatest in the center of the streamer, and causes the point of largest net remediation to move outward at early times.

amount of NO remediation occurs in the center of the streamer where the N density is the highest. At higher energy depositions and higher center line gas temperatures, processes such as Eq. (16) become significant. As a result, there is net NO generation at small radii, and net NO remediation at larger radii and lower gas temperatures.

IV. DIFFUSIVE AND ADVECTIVE TRANSPORT

In Sec. IV, we will examine NO remediation in the vicinity of microstreamers in DBD while including advection. In doing so, we have expanded the streamer radius from 10 to 30 μm. In order to minimize complications due to edge effects (e.g., reflection of acoustic waves) we have increased the computational area to 0.8×0.8 cm^2. The standard case is the same as that used in Sec. III with the exception that the streamer averaged energy deposition has been increased to 1130 mJ/cm^3 (0.05 mJ/cm^3 volume averaged).

The temperature rise in the streamer region resulting from the current pulse produces a pressure gradient which initiates radial advection. This conversion of the thermal energy of the gas into kinetic energy results in lower peak temperature rise than one would obtain when considering diffusion only. The gas temperature, mass density, and mass flux during and following the pulse are shown in Fig. 6. The energy deposition by the current pulse is over by $t\approx15$ ns, which produces peak on axis temperature rise of ≈150 K which is roughly that obtained in Sec. III. This generates a pressure gradient and initiates advection radially outward. Unlike the diffusion only cases, the advection of hot mass out of the streamer region, produces significantly increased temperatures at radii noticeably outside of the streamer region. The expansion wave generates a mass front akin to a weak blast wave which propagates radially outward. Once the power deposition ceases at the end of the pulse, the temperature begins to decrease by expansion cooling and thermal conduction. Mass continues to move radially outward due to both inertia and the still negative pressure gradient. The end result is a rarefaction wave.

Once the temperature has decreased sufficiently by conduction and expansion, the pressure gradient reverses resulting in an influx of mass back into the streamer region. The backward motion of the mass into the streamer region, the viscosity of the gas acting on the forward motion of the streamer, and the differential in temperature, and thus the internal energy, across the wave widen and flatten the wave, dissipating it as it moves out. The streamer region finally fills in due to cooling of the core and backstreaming of the gas. Advective motion at long times is mainly limited to small acoustic waves which propagate back and forth throughout the gas. The amplitude of these waves is small compared to the absolute density of the gas and they do not contribute significantly to changes in the gas density at these times.

The N atom and O_3 densities during and after a current pulse when including advection are shown in Fig. 7. NO and NO_2 densities are shown in Fig. 8. During the current pulse electrons are initially generated in the streamer region. Electron impact processes generate N atoms in the streamer region. Advection of ions and ambipolar diffusion of electrons during the somewhat longer current pulse produce electrons

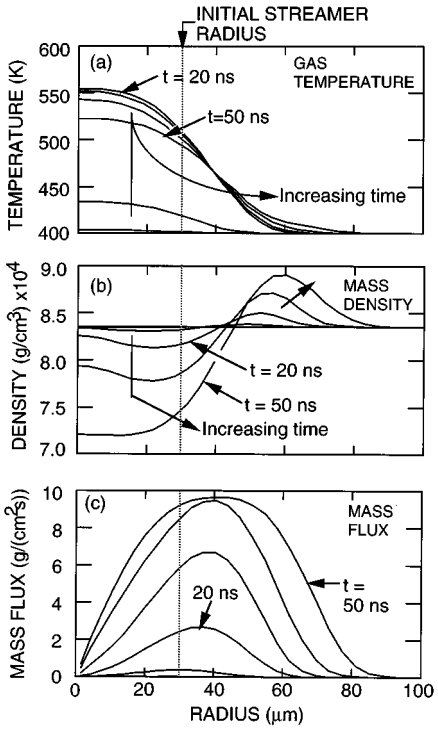

FIG. 6. Microstreamer characteristics when including advection during the first 50 ns. (a) Temperature, (b) mass density, and (c) mass flux (mass density$\times$velocity). The initial gas mixture is $N_2/O_2/H_2O=85/5/10$ (1 atm, 400 K, 10 kV) with 500 ppm of NO. The streamer–volume averaged energy deposition is 1130 mJ/cm^3 during a current pulse lasting 20 ns. The temperature is increased outside the streamer region due to thermal conduction and the motion of hot mass outward. A front of high mass density forms outside the streamer region due to advection from the core of the streamer. Flux is greatest outside the streamer region due to the larger temperature gradient there. The gas begins to cool immediately after the energy deposition has stopped.

by additional avalanche outside the initial streamer radius which generate N atoms by dissociation of N_2. There is more significant density of N atoms outside the initial streamer region due to both production and motion of N outward compared to the diffusion only case. Rapid consumption of N by reassociation and remediation reactions however restricts its range. The secondary radical O_3 has a qualitatively different shape than for the diffusion only case. Its density is maximum slightly off axis due in part to the rarefaction on axis and compression off axis of the mass density. When O is exhausted, the O_3 diffuses to larger radii.

The NO density initially decreases in the streamer region due to reduction reactions with N atoms and rarefaction resulting from advection. Reduction reactions continue until the N atom density is depleted at $\approx10^{-5}$ s. Note that the maximum NO density actually occurs at early times in the crest of the shock wave which results from the current impulse. The NO density in the streamer region continues to decrease after the depletion of N due to continued rarefaction in the core and reactions with O_3. At $\approx10^{-5}$–10^{-4} s, the density increases due to back diffusion and the inward directed flux resulting from the reversal in the pressure gradient. The degree of depletion of NO due to the advective transport and reactions with N will be discussed below.

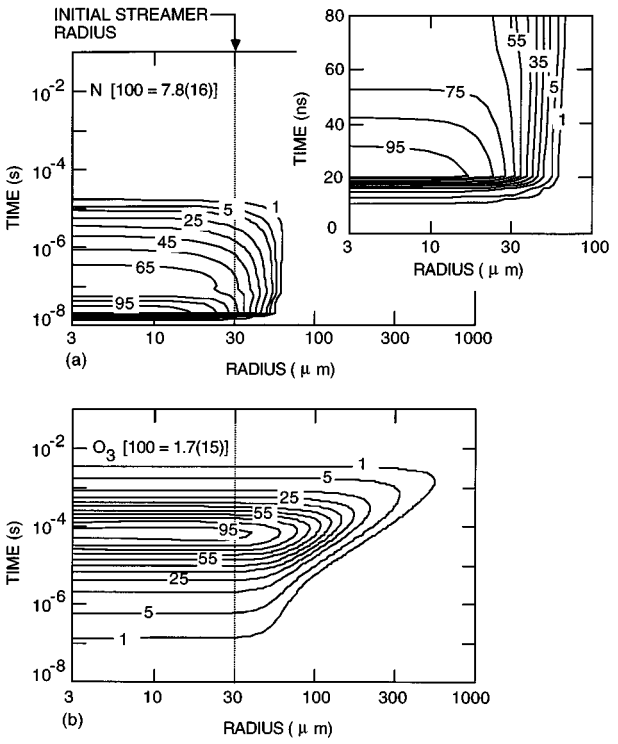

FIG. 7. Densities (cm^{-3}) of (a) N and (b) O_3 for the conditions of Fig. 6. The contours are labeled with the percentage of the maximum value indicated. The N atom density peaks on axis after the current pulse, prior to significant rarefaction. The O_3 density continues to increase until the O atoms are exhausted at $\approx 10^{-5}$ s, and have a small off axis peak due to rarefaction. The density later decreases due to diffusion to the bulk.

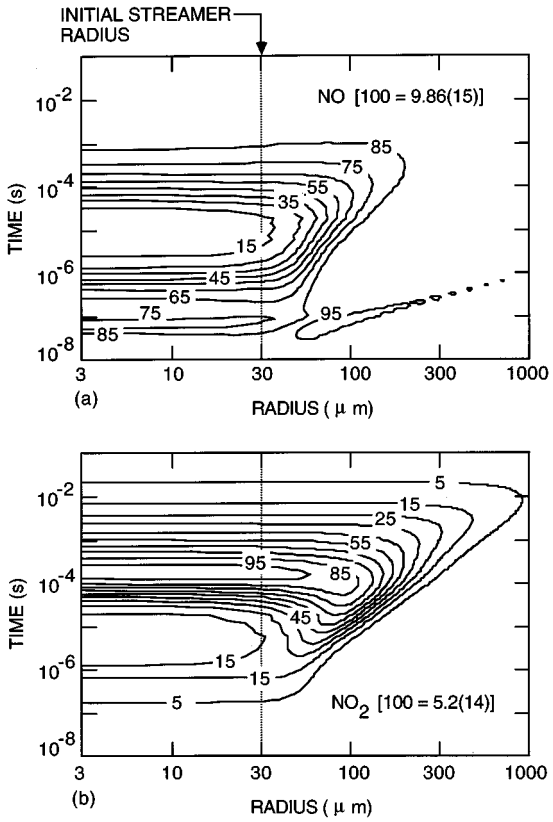

FIG. 8. Densities (cm^{-3}) of (a) NO and (b) NO_2 for the conditions of Fig. 6. The contours are labeled with the percentage of the maximum value indicated. The NO density is depleted on axis due to both remediation and rarefaction. Diffusion of NO from larger radii fills in the core at later times. Due to rarefaction of NO in the core, the NO_2 density first peaks off axis.

NO_2 is primarily generated at early times by reactions between O and NO. This production continues until the O is exhausted at $\approx 10^{-5}$ s. The depletion of NO in the streamer which occurs at near the same time also slows the production of NO_2. It also results in N being available to react with NO_2 [Eq. (12)] which regenerates a small amount of NO while depleting NO_2. The amount of NO produced in this way is not large compared to other channels but the reduction is significant for the NO_2. The depletion of NO in the streamer region also slows any depletion of O_3 on the axis since reaction with NO is a major depleting reaction. The rarefaction of the core and the abundance of both NO and O_3 outside the streamer region produces an off axis maximum in the density of NO_2 at $t \approx 10^{-4}$ s. As NO repopulates the core and reacts with O_3 the NO_2 density regains an on-axis maximum in its density ($t \simeq 3 \times 10^{-4}$ s). Finally, the NO_2 density is depleted by diffusion to larger radii.

On axis NO and N densities and the gas temperature are shown in Fig. 9 for streamer–volume averaged energy depositions of $\approx$23–1260 mJ/cm^3. The maximum on-axis N atoms and gas temperatures are shown in Fig. 10. Larger energy deposition generates larger densities of N atoms and more on axis depletion of NO by remediation and rarefaction. The gas temperatures have peak excursions of up to 155 K. Increasing temperatures result in production of NO in the streamer region by the $N+O_2$ reactions. This production is partly reflected by the local maximum in NO density at $\approx 10^{-7}$ s. The relative amounts of on axis NO depletion due to chemical reactions and rarefaction are in Fig. 10 where we show the amount of depletion of NO and mass density as a function of energy deposition. At the higher energy depositions, the depletion of NO nears unity, while rarefaction is $\approx$25%. The depletion of NO, seen to be largely by reduction, leaves unreacted N atoms which could recombine, thereby reducing the remediation efficiency. This occurs at a time when increasing energy deposition can also decrease remediation efficiency due to NO production at the higher temperatures. The increased advective motion which occurs at high energy deposition helps to offset this effect by moving more N atoms outside the streamer region to react with NO in the bulk gas. This acts to increase efficiency. The increased advective motion is shown in Fig. 11(a) where the mass densities are shown when the compression is maximum ($t \approx 50$–100 ns). The increasing advective motion and larger availability of N from the core due to depletion of NO at higher energy depositions results in removal of NO over a larger volume. For example, NO profiles are shown in Fig. 11(b) when the NO density reaches a minimum in the streamer region ($t \approx 1$ μs). Transport can therefore aid remediation in the following ways. First convection *increases* N/NO in the bulk gas which increases remediation since N is initially small there. Second, convection *decreases* N/NO in

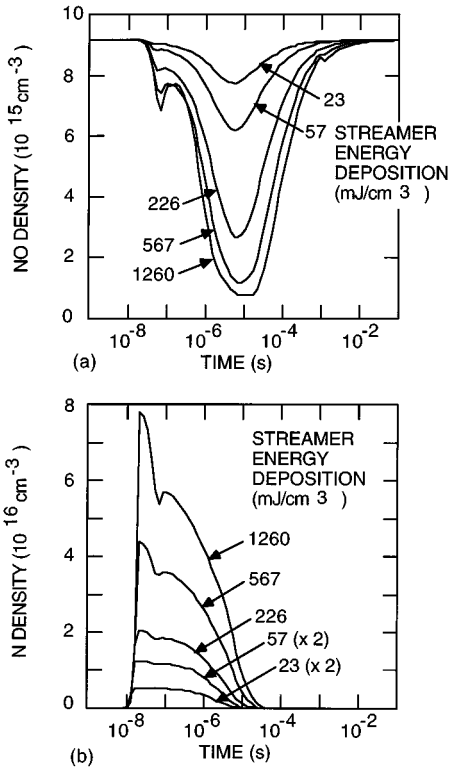

FIG. 9. Microstreamer properties on axis ($r=0$) for different streamer energy depositions. (a) NO density and (b) N atom density. At high energy deposition the reaction $N+O_2 \rightarrow NO+O$ replenishes the NO density at times of $\approx 10^{-7}$ s.

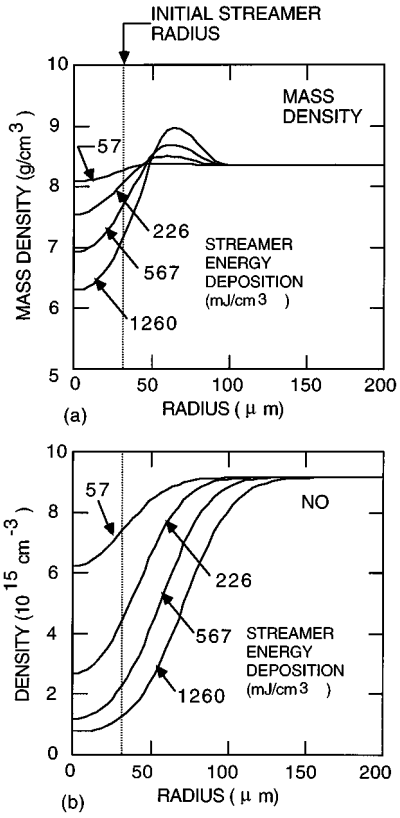

FIG. 11. Densities as a function of radius for different energy depositions. (a) Mass density at times corresponding to the peak in the rarefaction wave ($\approx$50–55 ns). (b) NO density at the time when the density is minimum on axis (7–10 μs). Increasing advective motion leads to depletion of NO over a larger volume with increasing energy deposition.

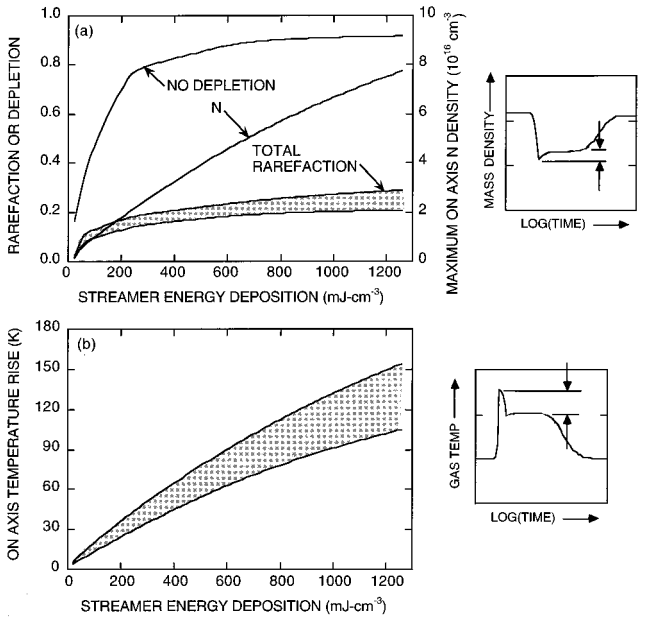

FIG. 10. On axis ($r=0$) properties as a function of streamer energy deposition. (a) Degree of rarefaction of NO and total mass density, and N atom density. (b) Gas temperature. The shaded region shows the range of values during the time when remediation is highest ($<10^{-4}$ s) as defined by the inset figures. Total rarefaction does not exceed 30%, whereas remediation reactions nearly totally deplete NO on the axis.

the streamer region which reduces loss of N due to reassociation since the absolute density of N is large there.

At high energy deposition, the increased temperature in the streamer which produces NO and the more favorable N/NO ratio as N moves farther out from the streamer region

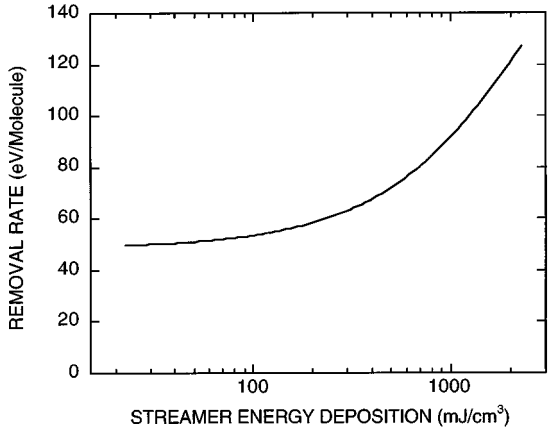

FIG. 12. Energy efficiency for N_xO_y as a function of streamer volume averaged energy deposition. Removal is less efficient with increasing energy deposition due to losses of N to reassociation and production of NO by increasingly accessible high activation energy processes.

into the bulk gas are competing processes with respect to energy efficiency. This trend is shown in Fig. 12 where efficiency is plotted in terms of eV required to remove all varieties of N_xO_y molecules. Removal is generally less efficient at higher energy depositions as N is increasingly used in reassociation rather than remediation and NO is generated at the higher temperatures.

V. CONCLUDING REMARKS

The filamentary plasmas in DBD devices generate radicals and deposit energy in a confined region. At high energy deposition, the local temperature rise can initiate advection. In low humidity atmospheric pressure gas streams, reduction of NO by N atoms generated by electron impact in the microstreamer is the dominant remediation process. If the N/NO ratio in the microstreamer is sufficiently large (either by large production of N or depletion of NO), the remediation efficiency may be low due to loss of N atoms to reassociation reactions. Convection of NO into the microstreamer from unprocessed volumes, and convection of N from the streamer region outwards improves remediation efficiency. This is accomplished by lowering the N/NO ratio in the streamer region and raising it in the bulk gas, and therefore increasing the fraction of N atoms which are consumed by reaction with NO (as opposed to reassociation). Large energy deposition which produces on axis temperature rises of hundreds °K, however, lower remediation efficiency by regenerating NO through reactions which have significant activation energy (such as $N+O_2 \rightarrow NO+O$). The end result is that remediation efficiency generally decreases with increasing energy deposition. The radial transport initiated by microstreamers which are initially tens of microns in diameter and lasting for a few to tens of ns extends to spatial scales of 0.1–1 cm for times of between tens and hundreds of ms. Given these observations, the optimum pulse format for uniform and highly efficient remediation of NO using DBDs will have a large area density ($10\ s\ cm^{-2}$) of low energy deposition pulses, producing temperature excursions of less than tens °K.

ACKNOWLEDGMENTS

This work was supported by the National Science Foundation (CTS94-12565) and the Office of Naval Research (N00014-94-1-0819). The authors thank Xudong Xu for his contributions to analysis of issues related to energy deposition.

[1] *Non-Thermal Plasma Technique for Pollution Control*, edited by B. M. Penetrante and S. E. Schultheis (Springer, Berlin, 1993), Parts A and B.
[2] I. Gallinberi, Pure Appl. Chem. **60**, 663 (1988).
[3] S. Masuda, Pure Appl. Chem. **60**, 727 (1988).
[4] L. Bromberg, D. R. Chon, M. Koch, R. M. Patrick, and P. Thomas, Phys. Lett. A **173**, 193 (1993).
[5] D. Evans, L. A. Rosocha, G. K. Anderson, J. J. Coogan, and M. J. Kushner, J. Appl. Phys. **74**, 5378 (1993).
[6] B. Eliason and U. Kogelschatz, IEEE Trans. Plasma Sci. **19**, 309 (1991).
[7] B. Eliason and U. Kogelschatz, Appl. Phys. B **46**, 299 (1988).
[8] B. Pashaie, S. K. Dhali, and F. I. Honea, J. Phys. D **27**, 2107 (1994).
[9] M. B. Chang, J. H. Balbach, M. J. Rood, and M. J. Kushner, J. Appl. Phys. **69**, 4409 (1991).
[10] A. C. Gentile and M. J. Kushner, J. Appl. Phys. **78**, 2074 (1995).
[11] W. D. Kimura, M. J. Kushner, E. A. Crawford, and S. R. Byron, Trans. Plasma Sci. **PS-14**, 246 (1986).
[12] A. C. Gentile, Ph.D. thesis (Chemical Physics), University of Illinois, Appendices A and B, 1995.
[13] P. A. Vitello, B. M. Penetrante, and J. N. Bardsley, Phys. Rev. E **49**, 5574 (1994).
[14] G. J. Pietch, D. Braun, and V. I. Gibalov, in *Proceedings of the NATO Advanced Research Workshop on Non-Thermal Plasma Techniques for Pollution Control*, edited by B. Penetrante and S. Schultheis (Springer, Berlin, 1993), pp. 273–286.
[15] J. O. Hirschfelder, C. F. Curtiss, and R. B. Bird, *Molecular Theory of Gases and Liquids* (Wiley, New York, 1954).
[16] A. C. Gentile, X. Xu, and M. J. Kushner, Gaseous Electronics Conference, Berkeley, CA, October 1995 (unpublished).
[17] J. Coogan and A. Sappey, Trans. Plasma Sci. (to be published).
[18] J. C. Person and D. O Ham, Radiat. Phys. Chem. **31**, 1 (1988).
[19] W. G. Mallard, F. Westley, J. T. Herron, and R. F. Hampson, *NIST Chemical Kinetics Database—Ver. 6.0* (NIST Standard Reference Data, Gaithersburg, MD, 1994).
[20] W. B. DeMore, D. M. Golden, R. F. Hampson, C. J. Howard, M. J. Kurylo, M. J. Molina, A. R. Ravishankara, and S. P. Sander, JPL Publication No. 87-41, Jet Propulsion Laboratory, California Institute of Technology, Pasadena CA, 1987.
[21] R. Atkinson, D. L. Baulch, R. A. Cox, R. F. Hampson, Jr., J. A. Kerr, and J. Troe, J. Phys. Chem. Ref. Data **18**, 881 (1989).